Optica Applicata, Vol. XXXIX, No. 4, 2009

Thermal model of nitride edge-emitting laser diodes

MACIEJ KUC*, ROBERT P. SARZAŁA

Laboratory of Computer Physics, Institute of Physics, Technical University of Łódź,
ul. Wólczańska 219, 90-924 Łódź, Poland

*Corresponding author: maciej.kuc@p.lodz.pl

Nitride laser diodes (LDs), as compared with arsenide ones, are known to exhibit poor thermal properties, mostly because of a very intense heat generation within their volumes. Therefore, to enable their useful operation, they should be designed in a way enhancing efficiency of heat-flux extraction from their volumes. In the present paper, the finite-element approach has been used to compare heat-flux spreading mechanism in continuous-wave room-temperature threshold operated nitride laser diodes with four different mounting schemes. For the standard laser width of 300 μm, the maximal active-region temperature increase over the RT ranges from 33.3 K (for the best two-sided heat LD mounting with the diamond heat spreader on the *p*-side) to 50.0 K (for the *n*-side LD mounting). As expected, laser diodes attached to their heat sinks on their *p*-side exhibit much more efficient heat-flux extraction than those attached on their *n*-type substrate. Even more efficient extraction takes place for the two-sided laser mounting. Besides, an application of the diamond heat spreader considerably enhances the above efficiency disregarding the place of its application. Further improvements may be expected in new optimised nitride laser devices designed in a way enhancing both heat-flux flow through areas of high-thermal-conductivity materials (diamond, copper, but also binary nitride compounds) and a reduction of heat-flux paths through layers of low-thermal-conductivity ternary and quaternary nitride compounds.

Keywords: InGaN/GaN laser diode, simulation of a laser diode operation, thermal model, heat-flux spreading analysis.

1. Introduction

From among all currently known semiconductor lasers, only nitride laser diodes manufactured with the aid of binary $A^{III}N$ compounds (*e.g.*, GaN, AlN and InN) and their possible ternary and quaternary compounds can emit radiation of short wavelengths from blue, violet and even ultraviolet parts of spectrum. Such laser devices may be applied in many areas of science, medicine, technology, entertainment, weapon, *etc*. But, in spite of desperate efforts made by numerous technological centers in the world, nitride lasers are still far from their anticipated commercial success. Market demand for reliable high-performance nitride lasers can reach even hundreds

of millions devices, however their performance is still not satisfactory. This is mostly connected with their insufficient thermal properties leading to a considerable increase in temperatures of their active regions which results in their insufficient lifetimes and output power.

Relatively poor thermal properties of nitride devices, as compared with arsenic ones, follow mostly from the fact of their active-region carrier transparency concentration being nearly ten times as high and the applied voltages being about twice as high. Therefore, thermal powers dissipated within nitride laser diodes (15–50 kW/cm^2 [1, 2] for their continuous-wave operation and even up to 375 kW/cm^2 [3] for their pulse operation) are about twenty times as high as those of arsenic ones. To reduce unwanted increases of temperature within a laser volume, such a high thermal power should be efficiently extracted from it, which requires an application of proper materials of high thermal conductivities and structures ensuring high extraction of a heat flux. Binary GaN, InN and AlN exhibit quite high thermal conductivities, however all nitride ternary and quaternary compounds suffer from very low thermal conductivity values. Therefore, more complex structures than in standard laser diodes have to be applied in nitride devices.

The main goal of this paper is to present a theoretical thermal model of nitride laser diodes and to use it to carry out a comparative analysis of thermal properties of their four possible mounting configurations.

2. Thermal conductivities of nitride materials

Thermal conductivities of nitride materials have been found to depend on the technology used, dislocation density, doping and sample sizes much more than it has been earlier measured for other $A^{III}B^{V}$ materials. For GaN, for example, its room-temperature (RT) values from 50 W/mK to 230 W/mK [4–7] have been reported. It has been determined to decrease with an increase in doping, for example, an increase in doping from 1.4×10^{18} cm^{-3} to 30×10^{18} cm^{-3} results in a decrease in its RT conductivity from 163 W/mK to 110 W/mK [4]. On the other hand, an increase in the thickness of the low-doped (4×10^{17} cm^{-3}) GaN sample from 200 μm to 2000 μm leads to an increase in its RT conductivity from 189 W/mK to 230 W/mK [6]. Besides, in bulk GaN crystals, doping has been found to have much less impact on their RT thermal conductivities [4, 7].

The above dependences are even more pronounced in the case of AlN, for which RT thermal conductivity in the broad range from as low as about 1 W/mK to as much as 285 W/mK has been reported [6, 8–11]. Its RT value, similarly to the case of GaN, depends on sample thickness and doping. Its highest RT value of 285 W/mK has been reported for the bulk AlN [8]. An increase in doping of relatively thick AlN samples (200 μm) from 4×10^{19} cm^{-3} to 30×10^{19} cm^{-3} results in a decrease in their RT thermal conductivity from 282 W/mK to 212 W/mK [5]. For much thinner samples, AlN RT thermal conductivity is considerably lower and is distinctly increased with an increase in their thickness [9, 10]. For its increase from 0.2 μm to 2.0 μm, for example, AlN

RT thermal conductivity has been increased from as low value as 1.8 W/mK to 76.5 W/mK [10].

Much less data are available for the thermal conductivity of InN. Only one measured result of its RT conductivity of 45 W/mK have been reported by KRUKOWSKI *et al*. [12].

There is an even more serious problem of finding in scientific literature reasonable values of thermal conductivities of various ternary nitride compounds as a function of their compositions. Only very scare experimental data are available. For example, PANTHA *et al*. [13] have found for 0.11-μm thick $In_yGa_{1-y}N$ the RT thermal conductivity decreasing from 8.10 W/mK to 1.05 W/mK for the mole fraction y of InN increased from 16% to 36%. DALY *et al*. [14] have measured analogous values of this parameter of 10 W/mK and 15 W/mK for $Al_{0.44}Ga_{0.56}N$ and $Al_{0.2}Ga_{0.8}N$ samples, respectively. However, in this case, sample thicknesses have been additionally changed from 0.04 μm to 0.09 μm. LIU and BALANDIN [15] have determined RT thermal conductivity of 25 W/mK for $Al_{0.4}Ga_{0.6}N$ sample of 0.7-μm thickness. Doping of the above samples has not been given.

Thermal resistivity, *i.e*., an inverse of the thermal conductivity $k(x)$, of the AB_xC_{1-x} ternary compound is usually presented as an weighted averaged of its values known for both composite binary AC and BC compounds corrected somewhat by a bowing parameter C_{ABC} [16]:

$$\frac{1}{k(x)} = \frac{x}{k_{AB}} + \frac{1-x}{k_{AC}} + x(1-x)C_{ABC}$$

with bowing parameter C_{ABC}. For the $Al_xGa_{1-x}N$ and $In_yGa_{1-y}N$ ternary compounds, the bowing parameters of 0.1 mK/W and 0.6 mK/W, respectively, have been found in [17]. For the quaternary $In_xAl_yGa_{1-x-y}N$ compound, the thermal conductivity has been estimated on the basis of its values for composite ternary compounds. Values of thermal conductivities used in the calculations are listed in Tab. 1. Thermal conductivity of nitride layers is known to depend not only on temperature but also on doping level. Besides, this parameter demonstrates distinct anisotropy because, for a vertical heat-flux flow, thermal conductivity is considerably reduced with a decrease in a layer thickness because of phonon scattering.

3. Laser structures

The analyzed laser structure has been reported in [18–22]. It is the edge-emitting (EEL) ridge-waveguide nitride laser emitting at RT the 411-nm radiation and grown with the aid of the plasma assisted molecular beam epitaxy (PAMBE) on the GaN substrate, which ensures very low density of possible misfit dislocations. The active region is in the form of three 3-nm intentionally undoped $In_{0.10}Ga_{0.90}N$ quantum-wells (QWs) separated by 7-nm $In_{0.02}Ga_{0.98}N$ barriers doped with Si to 5×10^{18} cm^{-3}. As electron blocking a 14 nm thick $In_{0.02}Al_{0.16}Ga_{0.82}N$ layer (EBL) is implemented. 70-nm

T a b l e 1. Composition, thicknes, doping and RT thermal conductivity k of successive layers of the ridge-waveguide edge-emitting (InGa)N quantum-well nitride diode laser under consideration. EBL – electron blocking layer, QW – quantum well.

	Laser element	Material	Thickness [nm]	Doping [cm^{-3}]	k_{RT} [W/mK] Lateral	k_{RT} [W/mK] Vertical
p-side	Metal contact	oxidized Au	2 030	–	317.1	317.1
		oxidized Ni	10	–	90.3	90.3
	Resistive layer	ZrO_x	200	–	1.35	1.35
	Capping layer	$In_{0.18}Ga_{0.82}N$	3	Mg: 4×10^{18}	8.7	2.0
	Contact layer	$In_{0.02}Ga_{0.98}N$	147	Mg: 4×10^{18}	51.0	18.9
p-type	Superlattice cladding	$In_{0.02}Ga_{0.98}N$	60×2.5	Mg: 2×10^{18}	2.0	0.7
		$In_{0.02}Al_{0.16}Ga_{0.82}N$	60×2.5	Mg: 2×10^{18}	2.0	0.7
	Waveguide	$In_{0.02}Ga_{0.98}N$	70	Mg: 2×10^{18}	51.6	17.5
	EBL	$In_{0.02}Al_{0.16}Ga_{0.82}N$	14	Mg: 4×10^{18}	40.4	11.3
Active region	QW	$In_{0.10}Ga_{0.90}N$	3×3	undoped	3.5	1.2
	Barrier	$In_{0.02}Ga_{0.98}N$	2×7	Si: 5×10^{18}		
n-type	Waveguide	$In_{0.02}Ga_{0.98}N$	100	undoped	55.8	19.5
	Buffer layer	GaN	40	undoped	211.6	65.6
	Cladding	$Al_{0.08}Ga_{0.92}N$	450	Si: 5×10^{18}	72.2	30.3
	Buffer layer	GaN	40	Si: 5×10^{18}	193.2	60.0
	Buffer	GaN	2 000	Si: 5×10^{18}	193.2	96.6
	Substrate	GaN	60 000	O: 5×10^{19}	179.4	134.6
n-side	Metal contact	Ti	30	–	22.0	22.0
		Au	2 070	–	317.1	317.1

n-type and 100-nm *p*-type $In_{0.02}Ga_{0.98}N$ waveguide layers are created on both sides of the active region. The active region with the waveguide is sandwiched by cladding layers: the 60-period $In_{0.02}Al_{0.16}Ga_{0.82}N/In_{0.02}Ga_{0.98}N$ superlattice *p*-type cladding and the 450-nm $Al_{0.08}Ga_{0.92}N$ *n*-type cladding. The *p*-type layers have been doped with magnesium, whereas the *n*-type ones – with silicon. The Ti/Au *n*-side and the oxidized Au/Ni *p*-side contacts have been applied. The 20-μm-wide and 300-nm-thick ridge waveguide is composed of the 3-nm $In_{0.18}Ga_{0.82}N$ (to reduce the contact resistance), 147-nm $In_{0.02}Ga_{0.98}N$ capping layers and a half of *p*-type superlattice (SL) cladding layer. Beyond the ridge area, the laser crystal is separated from the Au contact with the aid of the 200-nm ZrO_x isolated layer. More structural details may be found in Fig. 1 and Tab. 1. (InGa)N ternary layers (instead of simpler binary GaN ones) are used on the *p*-type laser side to decrease the activation energy of the Mg acceptor which results in higher layer electrical conductivities. Additionally, (InGa)N/(InAlGa)N superlattice increases the hole concentration.

The laser crystal is stuck on a 4-mm-thick copper heat sink with the aid of a 5-mm-thick In solder. The Peltier element has been assumed to be used to keep external surfaces of the copper heat sinks at a constant temperature of 293 K. A 300-μm-thick

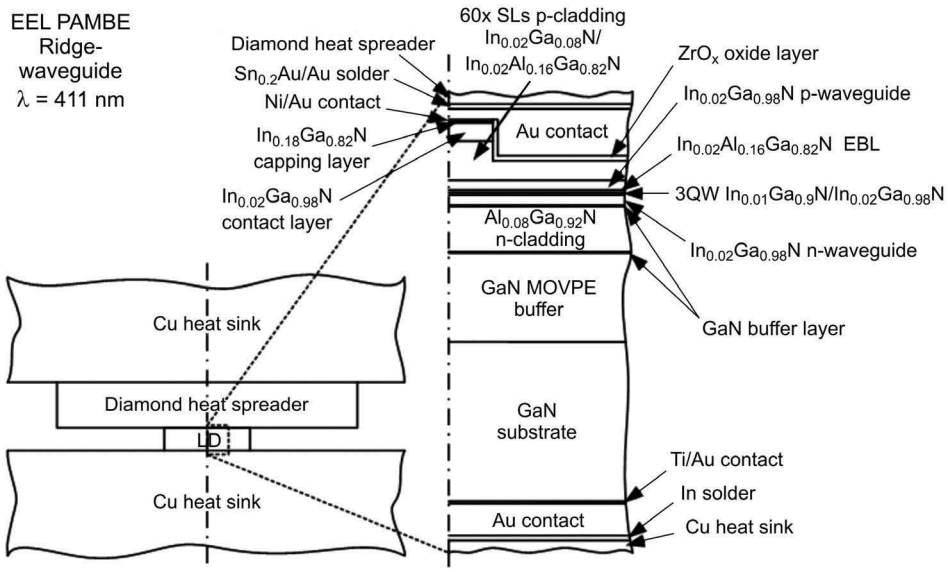

Fig. 1. Structure of the ridge-waveguide edge-emitting (EEL) (InGa)N quantum-well nitride laser diode attached from both sides to the copper heat sink and with the diamond heat spreader on the *p*-side. EBL – electron blocking layer, HS – heat sink, LD – laser diode, SL – superlattice.

diamond heat spreader is coated with 3 μm $Sn_{0.2}Au$ eutectic layer and extra 1 μm gold layer. Thermal conductivities of diamond and $Sn_{0.2}Au$ alloy were found to be 1120.0 W/mK [23] and correspondingly 57.3 W/mK [24] (Tab. 2). Anisotropy and temperature effects have been neglected for diamond and metallic layers.

T a b l e 2. Thickness and conductivity *k* of heat-sinking elements.

Heat-sinking element	Material	Thickness [μm]	k_{RT} [W/mK]
Heat sink	Cu	4 000	400.8
Heat sink solder	In	5	81.6
Heat spreader	Diamond	300	1120.0
Heat spreader solder	$Sn_{0.2}Au$	3	57.3
	Au	1	317.1

Diamond heat spreaders improve the cooling capability of LEDs [25], LDs [22] as well as LD arrays [26]. Four laser-diode (LD) mounting configurations shown in Fig. 2 are considered: *i*) *n*-side LD mounting (HS-nLD), *ii*) *p*-side LD mounting (HS-pLD), *iii*) *p*-side LD mounting with the diamond heat spreader (HS-Di-pLD), *iv*) two-sided LD mounting with the diamond heat spreader on its *p*-side (HS-Di-pLDn-HS). A configuration of heat-sinking elements and their sizes are given in Fig. 3.

For RT continuous-wave (CW) operation, both threshold current density j_{th} of 4.2 kA/cm^2 and threshold voltage V_{th} of 5.3 V have been determined for the laser under

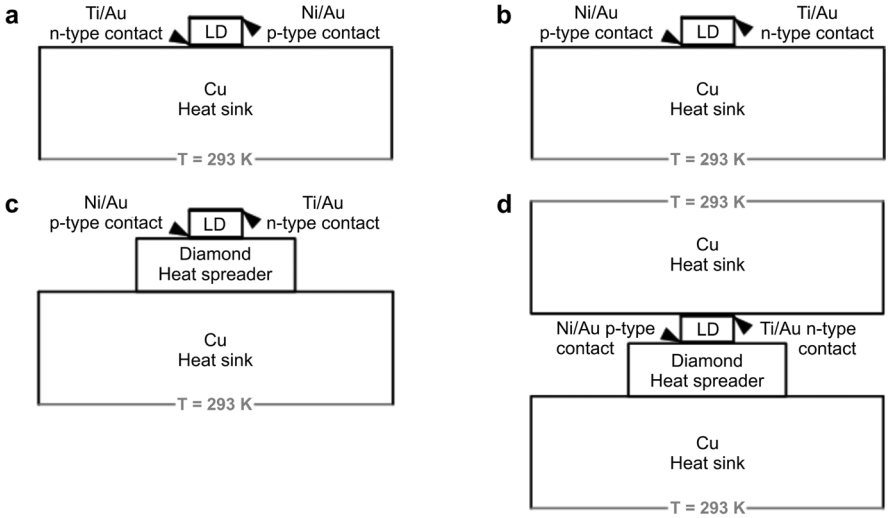

Fig. 2. Four heat-sinking LD configurations considered: *n*-side LD mounting (HS-nLD) – **a**, *p*-side LD mounting (HS-pLD) – **b**, *p*-side LD mounting with the diamond heat spreader (HS-Di-pLD) – **c**, two-sided LD mounting with the diamond heat spreader on the *p*-side (HS-Di-pLDn-HS) – **d**.

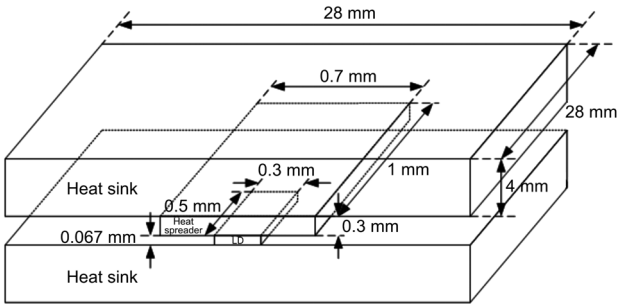

Fig. 3. Configuration and sizes of heat-sinking elements.

consideration. They are very low mostly because of relatively small electrical resistivities of the laser *p*-type layers.

4. Heat-flux spreading analysis

The finite-element method has been used to determine two-dimensional temperature profiles within the laser crystal as well as within both the copper heat sink and the diamond heat spreader. Heat source efficiency was extracted from the light-current--voltage characteristic for the laser structure analyzed. All external heat-sink, heat--spreader and laser-crystal surfaces have been regarded as thermally isolated, with an exception of the base of the copper heat sink for which, because of the attached Peltier element, a constant ambient temperature of 293.0 K has been assumed. All

temperature profiles presented have been found for the RT CW threshold laser operation (j_{th} = 4.2 kA/cm^2, V_{th} = 5.3 V).

As expected, for the four laser configurations considered, the highest temperature increase takes place within LD active regions. Its numerical values given below have been determined for structure sizes shown in Fig. 3. The maximal active-region temperature T_{max} of 343.0 K has been determined for the *n*-side laser crystal mounting (Fig. 2**a**), whereas the lowest T_{max} of only 326.3 K – for the two-sided LD mounting with the diamond heat spreader on the *p*-side (Fig. 2**d**). For the *p*-side LD mounting without (Fig. 2**b**) and with (Fig. 2**c**) the diamond heat spreader, the above T_{max} of 338.2 K and 337.4 K, respectively, has been calculated. Additionally, T_{max} of 338.5 K has been determined for the *n*-side LD mounting with the additional diamond heat spreader on its *p*-side (Fig. 4) – the HS-nLDp-Di configuration. This temperature is only somewhat higher than 338.2 K found for the *p*-side LD mounting (Fig. 2**b**), which confirms a considerable impact on heat-flux spreading process of the high-thermal-conductivity diamond crystal.

Diamond crystals of thermal conductivity considerably higher than those of other materials are often used to manage heating problems in electronic devices. Its role may be easily observed in Fig. 4, presenting heat-flux spreading within the HS-nLDp-Di laser as well as within its both copper heat sink and diamond heat-spreader. Directions of heat fluxes may be clearly studied analysing isotherms plotted in this figure. As expected, within the copper heat sink of sizes many times larger than those of a laser diode, the heat fluxes are directed approximately in radial directions leading for longer

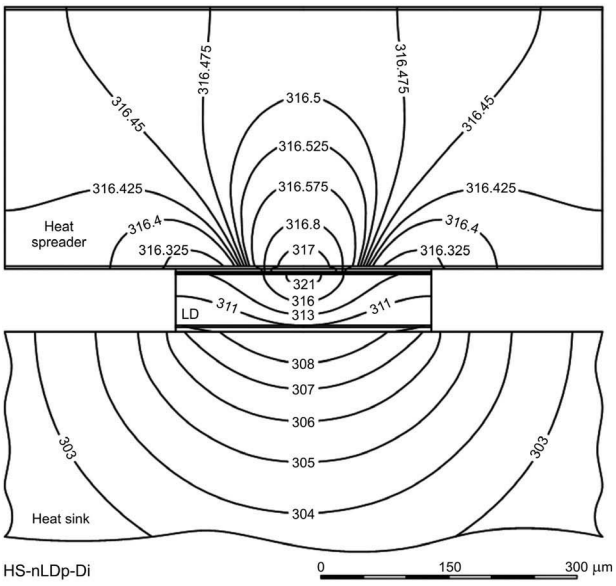

Fig. 4. Temperature isotherms determined for the RT CW threshold operation of the nitride laser diode *n*-side mounted to the copper heat sink and additionally equipped with the diamond heat spreader on its *p*-side (HS-nLDp-Di).

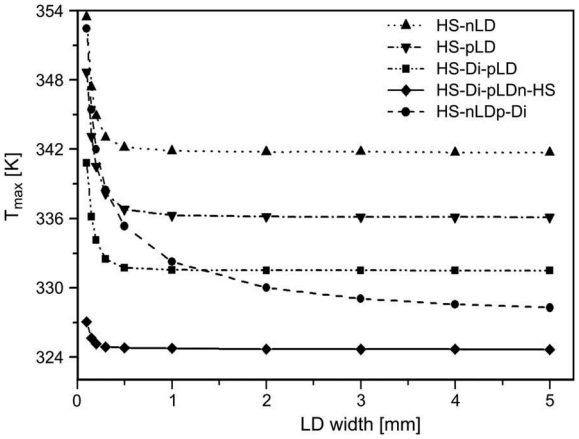

Fig. 5. Maximal active-region temperatures T_{max} determined for the RT CW threshold operation of the nitride laser diode for its various mounting configurations versus the width of the laser diode together with its heat spreader.

distances to nearly circular isotherms. Within the diamond heat spreader (note much smaller temperature differences between successive isotherms), on the other hand, heat fluxes are initially also directed radially from the LD centre but later they are turning back flowing through distant heat-spreader areas towards the LD crystal. Therefore, a much more uniform heat-flux enters the heat sink from the LD crystal than it could be expected for LD without the diamond heat spreader. Hence, because of this lateral heat-flux spreading within the diamond crystal, efficiency of the whole heat extraction process from the laser volume has been dramatically enhanced.

Figure 5 presents values of the maximal active-region temperatures T_{max} determined for the RT CW threshold operation of the nitride laser diode for its various mounting configurations versus the width of the laser diode together with its heat spreader. As expected, the LD configuration with two-sided heat extraction ensures the most efficient heat-flux extraction from the LD volume for all widths of its diamond heat spreader. Besides, for very wide LD widths, devices with the diamond heat spreader exhibit distinctly lower temperature increases, whereas, for the narrower ones, its profitable impact is steadily reduced. For laser diodes without the heat spreader, an increase in their widths over 0.3 mm practically does not have any influence on the heat extraction process.

5. Conclusions

Heat-flux spreading mechanism within laser crystal as well as within its heat spreader and heat sink for the room-temperature (RT) continuous-wave (CW) threshold operated nitride edge-emitting laser diode and its four different mounting schemes is analysed and compared. As expected, laser diodes attached to the copper heat sink on their *p*-side exhibit higher efficiency of heat-flux extraction from their volumes than

those attached on the *n*-type substrate. Besides, the diamond heat spreader for all of its places of application considered has been found to considerably enhance efficiency of the above heat-flux extraction. For the standard laser width of 300 μm (shown in Fig. 3), the maximal active-region temperature increase over the ambient temperature of 293 K ranges from 33.3 K (for the best two-sided heat LD mounting with the diamond heat spreader on the *p*-side) to 50.0 K (for the *n*-side LD mounting). Further improvements may be expected in new optimised laser devices designed in a way enhancing both efficient heat-flux flow through areas of high-thermal-conductivity materials (diamond, copper, but also binary nitride compounds) and a reduction of heat-flux paths through layers of low-thermal-conductivity ternary and quaternary nitride compounds.

Acknowledgements – The authors would like to acknowledge support from the Polish Ministry of Science and Higher Education (MNiSzW), grant POIG. 01. 03. 01-00-159/08.

References

[1] ASANO T., TOJYO T., MIZUNO T., TAKEYA M., IKEDA S., SHIBUYA K., HINO T., UCHIDA S., IKEDA M., *100-mW kink-free blue-violet laser diodes with low aspect ratio*, IEEE Journal of Quantum Electronics **39**(1), 2003, pp. 135–140.

[2] RYU H.Y., HA K.H., LEE S.N., JANG T., SON J.K., PAEK H.S., SUNG Y.J., KIM H.K., KIM K.S., NAM O.H., PARK Y.J., SHIM J.I., *High-performance blue InGaN laser diodes with single--quantum-well active layers*, IEEE Photonics Technology Letters **19**(21), 2007, pp. 1717–1719.

[3] CHO J., CHO S., KIM B.J., CHAE S., SONE C., NAM O.H., LEE J.W., PARK Y., KIM T.I., *InGaN/GaN multi-quantum well distributed Bragg reflector laser diode*, Applied Physics Letters **76**(12), 2000, pp. 1489–1491.

[4] FLORESCU D.I., ASNIN V.M., POLLAK F.H., MOLNAR R.J., WOOD C.E.C., *High spatial resolution thermal conductivity and Raman spectroscopy investigation of hydride vapor phase epitaxy grown n-GaN/sapphire (0001): Doping dependence*, Journal of Applied Physics **88**(6), 2000, pp. 3295–3300.

[5] SLACK G.A., SCHOWALTER L.J., MORELLI D., FREITAS JR. J.A., *Some effects of oxygen impurities on AlN and GaN*, Journal of Crystal Growth **246**(3–4), 2002, pp. 287–298.

[6] MION C., MUTH J.F., PREBLE E.A., HANSER D., *Accurate dependence of gallium nitride thermal conductivity on dislocation density*, Applied Physics Letters **89**(9), 2006, p. 092123.

[7] OSHIMA Y., YOSHIDA T., ERI T., SHIBATA M., MISHIMA T., *Thermal and electrical properties of high-quality freestanding GaN wafers with high carrier concentration*, Physica Status Solidi (c) **4**(7), 2007, pp. 2215–2218.

[8] SLACK G.A., TANZILLI R.A., POHL R.O., VANDERSANDE J.W., *The intrinsic thermal conductivity of AlN*, Journal of Physics and Chemistry of Solids **48**(7), 1987, pp. 641–647.

[9] KATO R., MAESONO A., TYE R.P., *Thermal conductivity measurement of submicron-thick films deposited on substrates by modified ac calorimetry (laser-heating Ångstrom method)*, International Journal of Thermophysics **22**(2), 2001, pp. 617–629.

[10] SUN ROCK CHOI, DONGSIK KIM, SUNG-HOON CHOA, SUNG-HOON LEE AND JONG-KUK KIM, *Thermal conductivity of AlN and SiC thin films*, International Journal of Thermophysics **27**(3), 2006, pp. 896–905.

[11] BONDOKOV R.T., MUELLER S.G., MORGAN K.E., SLACK G.A., SCHUJMAN S., WOOD M.C., SMART J.A., SCHOWALTER L.J., *Large-area AlN substrates for electronic applications: An industrial perspective*, Journal of Crystal Growth **310**(17), 2008, pp. 4020–4026.

[12] KRUKOWSKI S., WITEK A., ADAMCZYK J., JUN J., BOCKOWSKI M., GRZEGORY I., LUCZNIK B., NOWAK G., WROBLEWSKI M., PRESZ A., GIERLOTKA S., STELMACH S., PALOSZ B., POROWSKI S., ZINN P., *Thermal properties of indum nitride*, Journal of Physics and Chemistry of Solids **59**(3), 1998, pp. 289–295.

[13] PANTHA B.N., DAHAL R., LI J., LIN J.Y., JIANG H.X., POMRENKE G., *Thermoelectric properties of $In_xGa_{1-x}N$ alloys*, Applied Physics Letters **92**(4), 2008, p. 042112.

[14] DALY B.C., MARIS H.J., NURMIKKO A.V., KUBALL M., HAN J., *Optical pump-and-probe measurement of the thermal conductivity of nitride thin films*, Journal of Applied Physics **92**(7), 2002, pp. 3820–3824.

[15] LIU W., BALANDIN A. A., *Temperature dependence of thermal conductivity of $Al_xGa_{1-x}N$ thin films measured by the differential 3ω technique*, Applied Physics Letters **85**(22), 2004, pp. 5230–5232.

[16] NAKWASKI W., *Thermal conductivity of binary, ternary, and quaternary III–V compounds*, Journal of Applied Physics **64**(1), 1988, pp. 159–166.

[17] PIPREK J., *Nitride Semiconductor Devices: Principles and Simulation*, Wiley-VCH Verlag GmbH, Weinheim 2007, pp. 3–11.

[18] SKIERBISZEWSKI C., WIŚNIEWSKI P., SIEKACZ M., PERLIN P., FEDUNIEWICZ-ZMUDA A., NOWAK G., GRZEGORY I., LESZCZYŃSKI M., POROWSKI S., *60 mW continuous-wave operation of InGaN laser diodes made by plasma-assisted molecular-beam epitaxy*, Applied Physics Letters **88**(22), 2006, p. 221108.

[19] SKIERBISZEWSKI C., PERLIN P., GRZEGORY I., POROWSKI S., *Continuous-wave operation of blue InGaN laser diodes made by plasma-assisted MBE*, Proceedings of the 28th International Conference on the Physics of Semiconductors, July 24–28, 2006, Vienna, Austria, Springer-Verlag, pp. 1409–1410.

[20] SKIERBISZEWSKI C., PERLIN P., GRZEGORY I., WASILEWSKI Z. R., SIEKACZ M., FEDUNIEWICZ A., WIŚNIEWSKI P., BORYSIUK J., PRYSTAWKO P., KAMLER G., SUSKI T., POROWSKI S., *High power blue--violet InGaN laser diodes grown on bulk GaN substrates by plasma-assisted molecular beam epitaxy*, Semicondor Science and Technology **20**(8), 2005, pp. 809–813.

[21] SKIERBISZEWSKI C., WASILEWSKI Z.R., SIEKACZ M., FEDUNIEWICZ A., PERLIN P., WIŚNIEWSKI P., BORYSIUK J., GRZEGORY I., LESZCZYŃSKI M., SUSKI T., POROWSKI S., *Blue-violet InGaN laser diodes grown on bulk GaN substrates by plasma-assisted molecular-beam epitaxy*, Applied Physics Letters **86**(1), 2005, p. 011114.

[22] ŚWIETLIK T., FRANSSEN G., WIŚNIEWSKI P., KRUKOWSKI S., ŁEPKOWSKI S.P., MARONA L., LESZCZYŃSKI M., PRYSTAWKO P., GRZEGORY I., SUSKI T., POROWSKI S., PERLIN P., CZERNECKI R., BERING-STANISZEWSKA A., ELISEEV P.G., *Anomalous temperature characteristics of single wide quantum well InGaN laser diode*, Applied Physics Letters **88**(7), 2006, p. 071121.

[23] WOLTER S.D., BORCA-TASCIUC D.-A., CHEN G., GOVINDARAJU N., COLLAZO R., OKUZUMI F., PRATER J.T., SITAR Z., *Thermal conductivity of epitaxially textured diamond films*, Diamond and Related Materials **12**(1), 2003, pp. 61–64.

[24] ROBOGIANNAKIS P., KYRIAKIS-BITZAROS E.D., MINOGLOU K., KATSAFOUROS S., KOSTOPOULOS A., KONSTANTINIDIS G., HALKIAS G., *Heterogeneous integration technique of optoelectronic dies to CMOS circuits via metallic bonding*, Proceedings of the Electronics System-Integration Technology Conference, September 2006, Dresden, Germany, IEEE, pp. 328–333.

[25] PO HAN CHEN, CHING LIANG LIN, LIU Y.K., TE YUAN CHUNG, CHENG-YI LIU, *Diamond heat spreader layer for high-power thin-GaN light-emitting diodes*, IEEE Photonics Technology Letters **20**(10), 2008, pp. 845–847.

[26] TOMM J.W., GERHARDT A., ELSAESSER T., LORENZEN D., HENNIG P., *Simultaneous quantification of strain and defects in high-power diode laser devices*, Applied Physics Letters **81**(17), 2002, pp. 3269–3271.

Received June 19, 2009